JOURNAL OF Materials CHEMISTRY

An *in situ* structural study of the thermal decomposition reactions of the ammonium thiomolybdates, $(NH_4)_2Mo_2S_{12}\cdot 2H_2O$ and $(NH_4)_2Mo_3S_{13}\cdot 2H_2O$†

Simon J. Hibble* and Mark R. Feaviour

Department of Chemistry, University of Reading, Whiteknights, Reading, UK RG6 6AD

Received 5th April 2001, Accepted 26th June 2001
First published as an Advance Article on the web 31st August 2001

A combined *in situ* Mo K-edge extended X-ray absorption fine structure (EXAFS) and X-ray powder diffraction study has been carried out to follow the evolution of structure in the thermal decomposition of the ammonium thiomolybdates, $(NH_4)_2Mo_3S_{13}\cdot 2H_2O$ and $(NH_4)_2Mo_2S_{12}\cdot 2H_2O$, under nitrogen. Additional information on the course of the decomposition reactions has been obtained from thermogravimetric and differential thermal analysis, and from IR spectroscopy. Molybdenum–molybdenum bonded triangular units are found to persist in all the amorphous intermediate decomposition products of $(NH_4)_2Mo_3S_{13}\cdot 2H_2O$, and are also formed during the decomposition of $(NH_4)_2Mo_2S_{12}\cdot 2H_2O$. Structural models for the intermediates are presented. The final decomposition product in both cases is poorly crystalline MoS_2.

Introduction

The thermal decomposition reactions of ammonium thiomolybdates have attracted interest, because the final product when these materials are heated in an inert atmosphere is MoS_2, a material used widely as a lubricant,[1] in hydrodesulfurisation catalysts,[2,3] and a possible battery cathode material.[4] Some of the intermediates, for example, amorphous MoS_3, which is produced in the decomposition of $(NH_4)_2MoS_4$, and amorphous MoS_4, which is claimed to be produced in the decomposition of $(NH_4)_2Mo_2S_{12}\cdot 2H_2O$, have also been investigated as battery cathode materials in lithium batteries.[5,6]

We are particularly interested in the structure of amorphous and poorly crystalline transition-metal sulfides, and as part of this programme have used previously combined extended X-ray fine structure (EXAFS) and X-ray diffraction to study the decomposition reaction of $(NH_4)_2MoS_4$ under nitrogen *in situ*.[7] Here, we have extended this work to follow the structural changes which occur when $(NH_4)_2Mo_2S_{12}$ and $(NH_4)_2Mo_3S_{13}$ are heated under nitrogen. Using EXAFS to follow the course of the decomposition reactions is attractive, because we obtain structural information, bond lengths and coordination numbers for the intermediates. We are therefore able to discriminate between the different intermediate species suggested by others, who proposed structures which were inferred indirectly from the results of thermal analysis and IR spectroscopy. *In situ* studies have a number of advantages over studies carried out by quenching intermediates for subsequent investigation. These advantages include avoiding the difficulties and uncertainties inherent in quenching and isolating intermediates, and the fact that systematic errors should remain constant. The latter is particularly useful when EXAFS is used to follow the change in Mo–S and Mo–Mo coordination numbers in the decomposition reactions we study here.

The structure of the cluster anions $Mo_3S(S_2)_6^{2-}$ and $Mo_2(S_2)_6^{2-}$[8] are shown in Fig. 1. Fig. 2 shows the reaction scheme of Müller *et al.*,[9] who proposed that the Mo–Mo bonded triangles found in $(NH_4)_2Mo_3S_{13}$ are retained over the course of the reaction, and that the decomposition to MoS_2 proceeds topochemically. This scheme appears chemically reasonable. EXAFS studies enable us to test whether the proposed intermediates are formed.

The thermal decomposition of $(NH_4)_2Mo_2S_{12}$, which contains the cluster anion $Mo_2(S_2)_6^{2-}$[10] shown in Fig. 1, has been less widely studied than the other ammonium thiomolybdates. Brito *et al.* in their thermal decomposition study[11] suggest that "Mo_2S_{10}" is formed as an intermediate and Fedin *et al.* assert that MoS_4 is produced.[12] Khudorozhko *et al.* have carried out a theoretical study of the structure of MoS_4 and performed lithium intercalation experiments on MoS_4.[6] They claim that their theoretical study shows that no Mo–Mo bonds are present in MoS_4 and also explain its behaviour in lithium intercalation reactions. EXAFS studies can easily reveal whether Mo–Mo bonds are present in the intermediates, and we were especially interested in the nature of these intermediates since the two proposed compositions spanned that of the amorphous molybdenum sulfide, $MoS_{4.7}$, which we had previously prepared by the reaction of molybdenum carbonyl with sulfur.[13]

Recently, Tremel's group have investigated the thermal decomposition of the ammonium thiomolybdates, $(NH_4)_2Mo_2S_{12}\cdot nH_2O$ and $(NH_4)_2Mo_3S_{13}\cdot nH_2O$, to form MoS_2 and also the microstructure of the MoS_2 formed.[14] They concluded

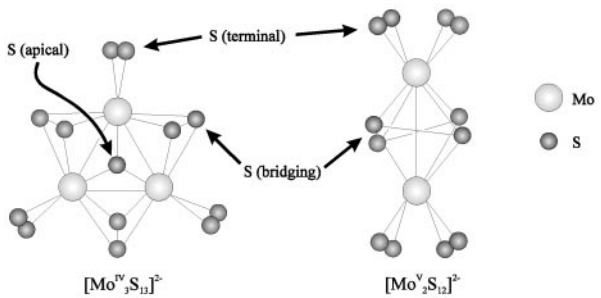

Fig. 1 The thiomolybdate anions, $Mo_3S(S_2)_6^{2-}$ and $Mo_2(S_2)_6^{2-}$.

†Electronic supplementary information (ESI) available: Table S1: structural parameters (model A) obtained from Mo K-edge EXAFS on heating $(NH_4)_2Mo_3S_{13}\cdot 2H_2O$ from 120 to 430 °C at 1 °C min^{-1}. Table S2: structural parameters (model A) obtained from Mo K-edge EXAFS on heating $(NH_4)_2Mo_2S_{12}\cdot 2H_2O$ from 100 to 450 °C at 1 °C min^{-1}. See http://www.rsc.org/suppdata/jm/b1/b103129p/

DOI: 10.1039/b103129p

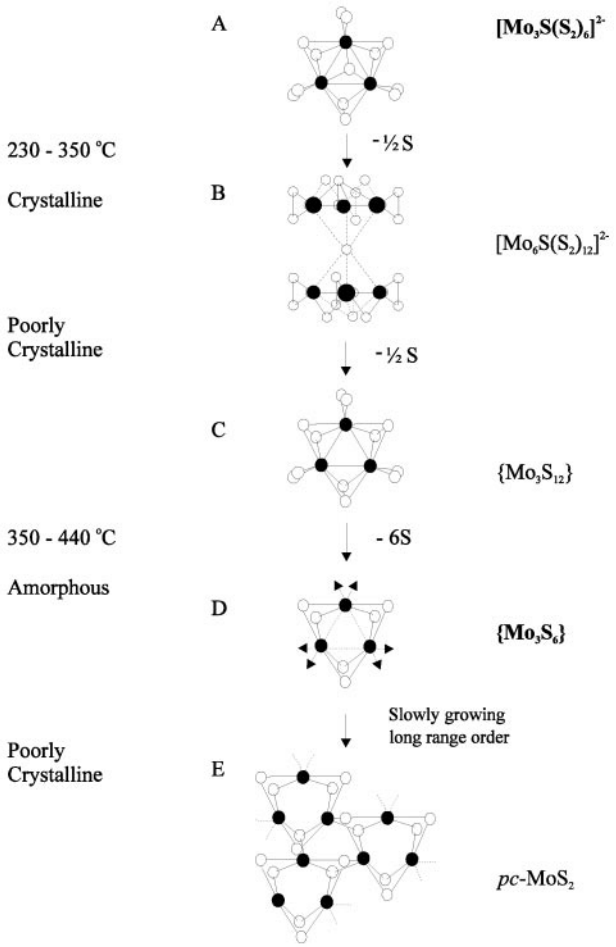

Fig. 2 A schematic representation of the thermal decomposition of $(NH_4)_2Mo_3S_{13}$ to poorly crystalline MoS_2 as described by Müller *et al.*,[9] filled circles are Mo and open circles S.

that the strongly exothermic peak occurring in the final step of the decomposition of $(NH_4)_2Mo_3S_{13}{\cdot}nH_2O$ to MoS_2 is a result of the topochemical nature of the reaction between Mo_3 units already present in the material, see Fig. 2. We thought it would be interesting to determine the identity of the units present before the final decomposition step in the formation of MoS_2 from both $(NH_4)_2Mo_3S_{13}{\cdot}nH_2O$ and $(NH_4)_2Mo_2S_{12}{\cdot}nH_2O$, and to follow in both cases the formation of poorly crystalline MoS_2 from the amorphous precursors using both EXAFS and X-ray diffraction.

Experimental section

Materials

$(NH_4)_2Mo_3S_{13}{\cdot}2H_2O$. This was prepared from $(NH_4)_6Mo_7O_{24}{\cdot}6H_2O$ (Lancaster) by the method outlined by Müller *et al.*[15] IR spectroscopy and powder X-ray diffraction confirmed the identity of the product as $(NH_4)_2Mo_3S_{13}{\cdot}2H_2O$.

$(NH_4)_2Mo_2S_{12}{\cdot}2H_2O$. $(NH_4)_2MoO_2S_2$ was prepared from $(NH_4)_6Mo_7O_{24}{\cdot}6H_2O$ (Lancaster) using the method of McDonald *et al.*[16] and converted to $(NH_4)_2MoO_2S_2$ by the method outlined by Müller *et al.*[15] IR spectroscopy and powder X-ray diffraction confirmed the product to be $(NH_4)_2Mo_2S_{12}{\cdot}2H_2O$.

IR spectroscopy. IR spectra were obtained from discs prepared by pressing a ground mixture of potassium bromide and the sample, and recorded using a Perkin-Elmer 1720-X interferometer.

Thermal analysis

Thermogravimetric analysis and differential thermal analysis were performed using a Stanton Redcroft STA 100 thermal analysis instrument.

The EXAFS/X-ray diffraction experiment

Combined EXAFS/XRD experiments were performed on Station 9.3 of the Daresbury SRS using experimental apparatus previously described.[17,18] The synchrotron source was operating with an average stored energy of 2 GeV and a typical electron current of 200 mA. EXAFS data were collected at the molybdenum K-edge ($E \approx 20\,000$ eV) in transmission mode from samples of $(NH_4)_2Mo_3S_{13}{\cdot}2H_2O$ and $(NH_4)_2Mo_2S_{12}{\cdot}2H_2O$. These were finely ground with boron nitride and pressed into 3 mm diameter pellets of around 1 mm thickness. The utility of boron nitride for this purpose is described in our earlier paper.[7] EXAFS data were collected in quick-EXAFS mode (QuEXAFS), using a rapidly scanning Si(220) monochromator, with the maximum k-value of the data limited to 16 Å^{-1}; this range of data was sufficient to allow detailed modelling of several atomic shells, but minimised the cycle time of the experiment. EXAFS data were calibrated using data collected from a molybdenum foil. Powder X-ray diffraction data were collected alternately with the EXAFS data using an X-ray wavelength of 1.0 Å. These data were collected for periods of slightly less than 5 min over a range $2\theta \approx 10$–$70°$. Diffraction patterns were collected using an INEL curved, position sensitive detector which was calibrated using a silicon standard. The combined time for an EXAFS scan, collection of an XRD pattern and associated monochromator movement was 10 min. Station 9.3 is equipped with a furnace which allows solid samples to be heated to 1000 °C and the temperature of the sample may be measured to within ±2 °C, using a thermocouple placed on the sample surface. All the experiments were performed under an atmosphere of flowing dry nitrogen and involved the rapid heating of the samples to 120 °C ($(NH_4)_2Mo_3S_{13}{\cdot}2H_2O$) and 70 °C ($(NH_4)_2Mo_2S_{12}{\cdot}2H_2O$) at 10 °C min^{-1}. The samples were then heated using a ramp rate of 1 °C min^{-1} until the temperature had reached 435 and 455 °C for the two samples. Owing to problems with the X-ray shutter malfunctioning, the first three EXAFS data sets were lost for $(NH_4)_2Mo_2S_{12}{\cdot}2H_2O$ and the first EXAFS data were collected at 100 °C. The same problem resulted in the loss of intensity seen in the two diffraction data sets collected at 170 and 310 °C during the decomposition of $(NH_4)_2Mo_3S_{13}{\cdot}2H_2O$ and the loss of the EXAFS data set which should have been collected at 240 °C. Fortunately, the problems did not have a significant impact on our experiment because they occurred at times when no structural changes were occurring.

Data analysis. The X-ray absorption data were normalised using the program EXCALIB.[19] The program EXBROOK[20] was used to carry out the pre-edge and post-edge subtraction to obtain the EXAFS signal $\chi(k)$. The EXAFS data were fitted in k-space with k^3-weighting from $k = 3$ Å^{-1} to $k = 16$ Å^{-1} using the program EXCURV98, which uses curved wave theory[21] and employs Hedin–Lindquist ground states and von Barth exchange potentials to calculate appropriate phase shifts. EXAFS spectra were Fourier transformed to produce a one-dimensional radial distribution function, using phase-shifts calculated for the first atomic shell.

Results

Thermal analysis

Fig. 3 shows the thermogravimetric and differential thermal analysis results for $(NH_4)_2Mo_3S_{13}{\cdot}2H_2O$ and $(NH_4)_2Mo_2S_{12}{\cdot}2H_2O$ heated under flowing nitrogen at 1 °C min^{-1}. The

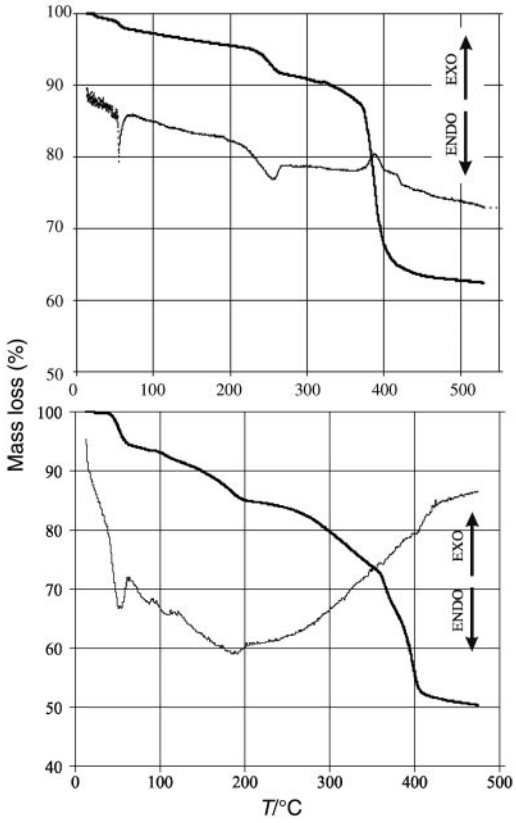

Fig. 3 The simultaneous TGA (bold) and DTA curves for the thermal decomposition of $(NH_4)_2Mo_3S_{13}\cdot 2H_2O$ (top) and $(NH_4)_2Mo_2S_{12}\cdot 2H_2O$ (bottom) at 1 °C min^{-1} in flowing N_2.

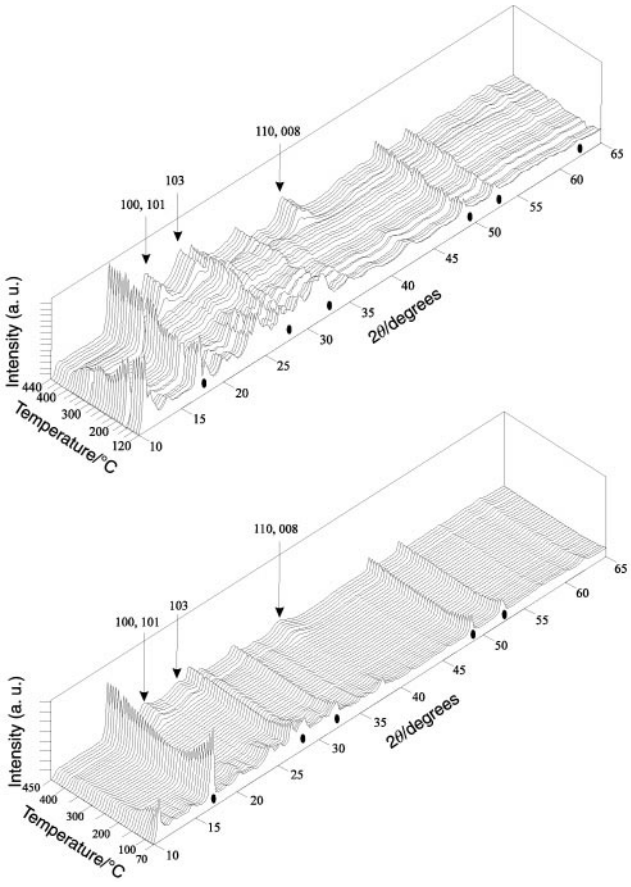

Fig. 4 The X-ray powder diffraction patterns ($\lambda = 1$ Å), recorded as $(NH_4)_2Mo_3S_{13}\cdot 2H_2O$ (top) was heated from 120 to 450 °C, and $(NH_4)_2Mo_2S_{12}\cdot 2H_2O$ (bottom) was heated from 70 to 450 °C, both at a heating rate of 1 °C min^{-1}. Peaks marked with • are due to the diluent crystalline boron nitride. The Bragg reflections from 2H-MoS_2 are labelled with their Miller indices.

same heating rate was used in the *in situ* EXAFS/XRD experiment after initially heating more rapidly to 120 °C ($(NH_4)_2Mo_3S_{13}\cdot 2H_2O$) and 70 °C ($(NH_4)_2Mo_2S_{12}\cdot 2H_2O$) at 10 °C min^{-1}. These results are in good agreement with those of other workers.[9,11,14] The principal differences are that the mass changes generally occur at lower temperatures in our experiment because of the slow heating rate employed. $(NH_4)_2Mo_2S_{12}\cdot 2H_2O$ loses both water molecules at about 60 °C, $(NH_4)_2Mo_3S_{13}\cdot 2H_2O$ loses one water molecule at about 60 °C followed by a more gradual loss of the second water molecule over the temperature range 60–200 °C. Dehydration is in each case followed by a number of steps that can be ascribed to loss of NH_3, H_2S and S, see Tables 1 and 2.

X-Ray diffraction

The X-ray diffraction patterns recorded during the decomposition of the ammonium thiomolybdate, $(NH_4)_2Mo_3S_{13}\cdot 2H_2O$, are shown in Fig. 4. These show that there is little change to the structure of the thiomolybdate up to 200 °C, consistent with the loss of only water of crystallisation. Appreciable crystallinity is retained to 300 °C with traces of crystallinity, see, for example, the Bragg peak at low angle,

Table 1 Thermal analysis data for the decomposition of $(NH_4)_2Mo_2S_{12}\cdot 2H_2O$ at 1 °C min^{-1} in flowing N_2

T/°C	Experimental mass loss (%)	*M*/g mol^{-1} product	Possible products	Calculated mass loss (%)	Possible loss
RT	0.0	648.0	$(NH_4)_2Mo_2S_{12}\cdot 2H_2O$	0.0	—
40–70	5.8	610.4	$(NH_4)_2Mo_2S_{12}$	5.6	$2H_2O$
100–200	15.0	550.8	$(NH_4)_2Mo_2S_{10}$	15.4	2S
200–360	27.0	473.0	Mo_2S_9	26.2	H_2S+2NH_3
360–450	49.0	330.5	Mo_2S_4 ($2MoS_2$)	50.6	5S

Table 2 Thermal analysis data for the decomposition of $(NH_4)_2Mo_3S_{13}\cdot 2H_2O$ at 1 °C min^{-1} in flowing N_2

T/°C	Experimental mass loss (%)	*M*/g mol^{-1} product	Possible products	Calculated mass loss (%)	Possible loss
20	0.0	776.6	$(NH_4)_2Mo_3S_{13}\cdot 2H_2O$	—	—
20–200	4.6	740.0	$(NH_4)_2Mo_3S_{13}$	4.6	$2H_2O$
200–280	8.7	706.6	$(NH_4)Mo_3S_{12.5}$	9.0	$½H_2S+NH_3$
280–370	12.8	672.5	Mo_3S_{12}	13.3	$½H_2S+NH_3$
370–530	37.2	485.0	Mo_3S_6 ($3MoS_2$)	38.1	6S

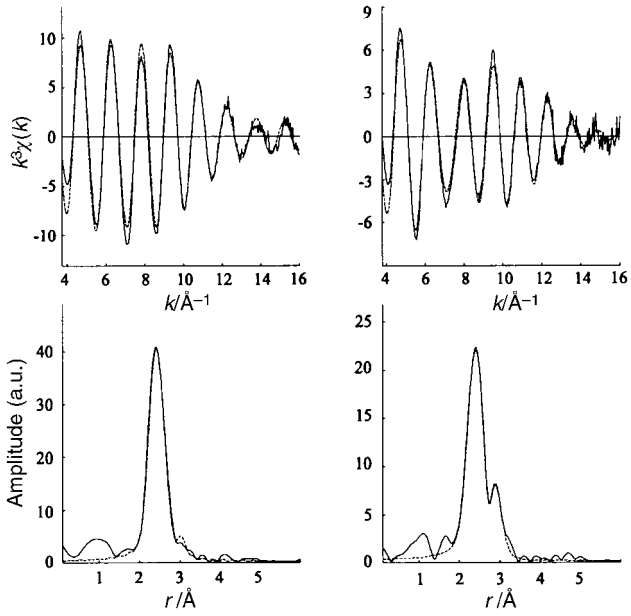

Fig. 5 Mo K-edge spectra (top) and their Fourier transforms (bottom) of the thermal decomposition product of $(NH_4)_2Mo_2S_{12}\cdot 2H_2O$ at 100–105 °C (left) and 340–345 °C (right). [—] experimental, [---] theoretical.

~11°, remaining until the Bragg peaks due to MoS_2 begin to appear at 360 °C. This supports the topotactic nature of the decomposition reaction of $(NH_4)_2Mo_3S_{13}$ to form MoS_2.

In contrast, X-ray diffraction patterns recorded during the decomposition of the ammonium thiomolybdate, $(NH_4)_2Mo_2S_{12}\cdot 2H_2O$, Fig. 4, show that all traces of crystallinity are lost as the temperature reaches 150 °C. This suggests that a major structural change is occurring at this temperature. Bragg peaks due to the formation of MoS_2 begin to appear at 370 °C.

EXAFS

Model A. The Mo K-edge EXAFS data were first analysed (Model A) using a two-shell model in which seven parameters (N_s, r_s, A_s, N_{Mo}, r_{Mo}, A_{Mo}, and E_0) were used in the least-squares refinement for the majority of the data sets. However, it was necessary to add an extra Mo shell for the temperatures at which both the precursor and MoS_2 coexisted, giving a maximum of ten parameters. Clear changes in Mo–S, Mo–Mo distances and coordination numbers, which were associated with the different stages of decomposition observed in the thermal analysis of $(NH_4)_2Mo_3S_{13}\cdot 2H_2O$ and $(NH_4)_2Mo_2S_{12}\cdot 2H_2O$, could be seen. Fig. 5 shows the fitted EXAFS signal, its Fourier transform for $(NH_4)_2Mo_2S_{12}$ at 100 °C and its decomposition product at 340 °C. For both thiomolybdates, EXAFS analysis showed that MoS_2 began to be formed at 350 °C. The full results are available as electronic supplementary information.†

The molybdenum–sulfur and molybdenum–molybdenum distances determined by EXAFS for the cluster anions present at the start of the reaction were in excellent agreement with those previously determined by X-ray crystallography[8,10] and sulfur coordination values also lay within the errors expected from EXAFS determination. However, the molybdenum coordination numbers determined were significantly lower than they should be for the starting materials. This problem is not unusual in EXAFS analysis and arises in part because of the high correlation between coordination number (N) and Debye–Waller factor (A). To overcome this problem we adopted the procedure below:

Table 3 Structural parameters (Model B) obtained from Mo K-edge EXAFS on heating $(NH_4)_2Mo_3S_{13}\cdot 2H_2O$ from 120 to 430 °C at 1 °C min^{-1}

T/°C	N_S	r_S/Å	A_S/Å^2	N_{Mo}	r_{Mo}/Å	A_{Mo}/Å^2	R (%)	N_p
120	6.60(31)	2.438(3)	0.012(1)	2.04(10)	2.735(2)	*0.0091*	16.63	6
130	6.91(33)	2.440(3)	0.013(1)	2.20(10)	2.735(2)	*0.0093*	19.60	6
140	6.89(34)	2.438(3)	0.013(1)	2.17(11)	2.735(2)	*0.0095*	20.18	6
150	6.89(34)	2.439(3)	0.013(1)	2.20(11)	2.735(2)	*0.0097*	19.71	6
160	6.70(34)	2.438(3)	0.013(1)	2.17(11)	2.736(3)	*0.0100*	19.37	6
170	6.94(39)	2.440(4)	0.014(1)	2.22(13)	2.736(3)	*0.0102*	23.29	6
180	6.88(35)	2.439(3)	0.014(1)	2.21(12)	2.736(3)	*0.0104*	20.85	6
190	6.85(36)	2.439(3)	0.014(1)	2.25(12)	2.736(3)	*0.0106*	21.36	6
200	6.78(34)	2.438(3)	0.014(1)	2.20(14)	2.736(3)	*0.0108*	22.56	6
210	6.68(38)	2.437(4)	0.015(1)	2.19(13)	2.736(3)	*0.0110*	23.40	6
220	6.51(32)	2.436(3)	0.014(1)	2.12(11)	2.734(3)	*0.0112*	21.20	6
230	6.44(36)	2.436(4)	0.015(1)	2.15(12)	2.733(3)	*0.0115*	23.00	6
250	6.39(36)	2.435(4)	0.015(1)	2.17(13)	2.735(3)	*0.0117*	24.23	6
260	6.31(34)	2.436(3)	0.015(1)	2.18(12)	2.734(3)	*0.0119*	23.28	6
270	6.31(35)	2.436(4)	0.015(1)	2.17(13)	2.735(3)	*0.0121*	23.95	6
280	6.16(31)	2.435(3)	0.015(1)	2.16(12)	2.733(3)	*0.0123*	21.98	6
290	6.13(30)	2.435(3)	0.015(1)	2.16(12)	2.734(3)	*0.0125*	21.66	6
300	5.98(29)	2.434(3)	0.015(1)	2.10(12)	2.734(3)	*0.0127*	21.56	6
310	6.25(39)	2.435(4)	0.016(1)	2.24(15)	2.734(4)	*0.0130*	26.65	6
320	6.04(32)	2.435(3)	0.016(1)	2.17(13)	2.734(3)	*0.0132*	23.09	6
330	6.09(30)	2.435(3)	0.016(1)	2.18(12)	2.734(3)	*0.0134*	21.51	6
340	6.11(38)	2.435(4)	0.017(1)	2.17(15)	2.735(3)	*0.0136*	27.26	6
350	5.43(30)	2.431(4)	0.015(1)	1.89(15)	2.735(3)	*0.0138*	23.84	9
				0.12(45)	3.164(7)	0.012(3)		
360	5.26(31)	2.421(4)	0.014(1)	1.32(17)	2.736(7)	*0.0140*	25.91	9
				0.95(55)	3.165(4)	0.013(3)		
370	5.10(27)	2.408(4)	0.011(1)	2.95(64)	3.167(5)	0.015(2)	24.34	7
380	5.25(26)	2.408(3)	0.011(1)	3.83(66)	3.173(5)	0.016(2)	22.34	7
390	5.35(30)	2.407(4)	0.011(1)	3.73(74)	3.172(5)	0.016(2)	26.00	7
400	5.32(29)	2.407(4)	0.011(1)	3.61(70)	3.172(5)	0.015(2)	25.33	7
410	5.28(30)	2.407(4)	0.011(1)	3.79(71)	3.172(5)	0.015(2)	25.91	7
420	5.27(30)	2.407(4)	0.012(1)	3.50(73)	3.173(5)	0.015(2)	26.87	7
430	5.57(27)	2.405(3)	0.012(1)	4.03(68)	3.172(4)	0.017(2)	21.03	7

N = Coordination number, r = interatomic distance, A = Debye–Waller factor, R = discrepancy index and N_p = number of independent parameters refined. Note: no errors are quoted for A_{Mo} for the Mo shell at *ca.* 2.7 Å (values in italics above) for the temperature range 120–360 °C because they were calculated using eqns. (1) and (2) (see text).

Model B. Determination of coordination numbers would be much more accurate if $A=2\sigma^2$ were known or could be reliably estimated. For both starting materials we knew N_{Mo} and by fixing this in the least-squares refinement we obtained A_{Mo} at the temperature at which the first EXAFS data were collected. We then used the relationships

$$\sigma = 4.106\left(\frac{1}{\mu\tilde{\nu}}\coth\left(\frac{x}{2}\right)\right)^{1/2} \quad (1)$$

$$x = 1.441\left(\frac{\tilde{\nu}}{T}\right) \quad (2)$$

where T = Temperature (K), μ = reduced mass, $\tilde{\nu} = \nu$(Mo–Mo) stretching vibration (wavenumbers), to determine A.[22] For $(NH_4)_2Mo_3S_{13}\cdot nH_2O$ at 300 K, eqn. (1) gives a value of $\tilde{\nu}_{Mo-Mo} = 210\ cm^{-1}$ in good agreement with Fedin *et al.*'s detailed vibrational spectroscopic study of $(NH_4)_2Mo_3S_{13}\cdot nH_2O$, in which they report $\tilde{\nu}_{Mo-Mo}$ contributions in the bands observed in the region 170–340 cm^{-1}.[23] The derived value of $\tilde{\nu}_{Mo-Mo}$ was used to calculate A_{Mo} over the temperature range 120–360 °C and was incorporated in our EXAFS analysis to produce model B. At temperatures higher than 350 °C, when model A suggests the formation of *pc*-MoS_2, the parameters were again refined independently and simultaneously, because there is little difference between experimental and calculated values of A_{Mo}. In the range 350–360 °C, A_{Mo} was calculated for the shell at 2.73 Å and obtained through least-squares refinements for the shell at 3.17 Å. The results are given in Table 3. For $(NH_4)_2Mo_2S_{12}$, we obtained $\tilde{\nu}_{Mo-Mo} = 175\ cm^{-1}$ from analysis of the 100 °C data set. The smaller value of $\tilde{\nu}_{Mo-Mo}$ is consistent with a weaker Mo–Mo bond in the Mo^{V} compound. In an intermediate stage of EXAFS analysis, which there is not space to report in detail here, we used A_{Mo} calculated from $\tilde{\nu}_{Mo-Mo} = 175\ cm^{-1}$ to fit to our data. This analysis revealed that the Mo^{V} containing starting material decomposes to form Mo^{IV} containing species, and that the most appropriate value of A_{Mo} to use is that calculated from the $(NH_4)_2Mo_3S_{13}$ EXAFS data. The results of EXAFS analysis for $(NH_4)_2Mo_2S_{12}$ and its decomposition products, calculated using A_{Mo} values appropriate to Mo_3 clusters (Model B), are given in Table 4.

$(NH_4)_2Mo_3S_{13}\cdot 2H_2O$. Fig. 6 (top) shows the behaviour of the average coordination numbers of molybdenum (N_{Mo}) and sulfur (N_S) around molybdenum in $(NH_4)_2Mo_3S_{13}\cdot 2H_2O$ and its decomposition products as a function of temperature using Model B to fit the EXAFS data. The Mo–Mo coordination number, for molybdenum at $d_{Mo-Mo} \sim 2.73$ Å, remains close to two over the temperature range 120–340 °C, which is consistent with the persistence of Mo–Mo triangles up to the point where MoS_2 begins to form at 350 °C. The behaviour of the Mo–S coordination number is more complex, remaining about 7, the value found in the complex ion $Mo_3S_{13}^{2-}$ up to 200 °C, when it begins to fall. The fall in the Mo–S coordination number above 200 °C is consistent with the loss of the apical triply-bridging sulfur from the cluster ion, $Mo_3S_{13}^{2-}$ (Fig. 1), and the loss of NH_3 and H_2S. It suggests that the condensation of two complex ions *via* six-coordinate sulfur, which was postulated by Müller *et al.*,[9] does not occur, because in this case the Mo–S coordination number would remain at 7. The Mo–S coordination number continues to fall to around 6 at 300 °C, consistent with

Table 4 Structural parameters (Model B) obtained from Mo K-edge EXAFS on heating $(NH_4)_2Mo_2S_{12}\cdot 2H_2O$ from 100 to 450 °C at 1 °C min^{-1}

T/°C	N_S	r_S/Å	A_S/Å^2	N_{Mo}	r_{Mo}/Å	A_{Mo}/Å^2	R (%)	N_p
100	7.21(27)	2.449(3)	0.011(1)	0.66(10)	2.826(7)	*0.009*	21.03	6
110	7.21(28)	2.448(3)	0.011(1)	0.62(10)	2.818(8)	*0.009*	21.83	6
120	7.11(33)	2.449(3)	0.011(1)	0.65(13)	2.822(9)	*0.0091*	27.12	6
130	7.12(34)	2.449(3)	0.012(1)	0.61(13)	2.816(10)	*0.0093*	28.16	6
140	6.88(33)	2.447(3)	0.012(1)	0.71(13)	2.810(8)	*0.0095*	27.58	6
150	6.62(31)	2.448(3)	0.012(1)	0.66(12)	2.805(9)	*0.0097*	26.47	6
160	6.35(31)	2.447(4)	0.012(1)	0.78(12)	2.799(7)	*0.0100*	27.57	6
170	5.98(29)	2.446(4)	0.013(1)	0.91(11)	2.791(6)	*0.0102*	25.88	6
180	5.88(35)	2.444(4)	0.014(1)	1.06(13)	2.784(6)	*0.0104*	31.22	6
190	5.71(34)	2.443(4)	0.014(1)	1.07(13)	2.777(6)	*0.0106*	30.72	6
200	5.76(34)	2.443(4)	0.014(1)	1.10(13)	2.775(6)	*0.0108*	30.10	6
210	5.74(33)	2.441(4)	0.014(1)	1.12(12)	2.770(5)	*0.0110*	28.25	6
220	5.85(38)	2.441(5)	0.014(1)	1.24(14)	2.767(6)	*0.0112*	32.48	6
230	5.84(35)	2.440(5)	0.015(1)	1.16(13)	2.763(6)	*0.0115*	29.40	6
240	5.96(38)	2.440(5)	0.015(1)	1.31(15)	2.757(5)	*0.0117*	30.19	6
250	5.95(37)	2.438(4)	0.015(1)	1.37(14)	2.758(5)	*0.0119*	30.10	6
260	5.79(35)	2.440(4)	0.015(1)	1.43(14)	2.757(5)	*0.0121*	29.49	6
270	5.84(36)	2.438(5)	0.015(1)	1.40(15)	2.752(5)	*0.0123*	30.36	6
280	5.83(38)	2.438(5)	0.015(1)	1.53(16)	2.749(5)	*0.0125*	31.11	6
290	5.75(37)	2.437(5)	0.015(1)	1.57(16)	2.746(5)	*0.0127*	31.39	6
300	5.63(34)	2.436(4)	0.015(1)	1.62(15)	2.743(5)	*0.0130*	29.06	6
310	5.52(31)	2.436(4)	0.015(1)	1.62(14)	2.746(4)	*0.0132*	27.17	6
320	5.51(33)	2.436(4)	0.015(1)	1.76(15)	2.743(4)	*0.0134*	29.54	6
330	5.54(34)	2.435(4)	0.015(1)	1.75(16)	2.740(5)	*0.0136*	29.84	6
340	5.49(37)	2.433(5)	0.016(1)	1.70(17)	2.743(5)	*0.0138*	22.55	6
350	5.47(38)	2.432(5)	0.016(1)	1.69(18)	2.743(6)	*0.0140*	29.80	6
360	5.07(28)	2.427(4)	0.015(1)	1.40(15)	2.741(5)	*0.0143*	25.20	9
				0.58(20)	3.169(8)	0.012(2)		
370	5.06(32)	2.418(4)	0.013(1)	0.98(19)	2.742(10)	*0.0145*	28.20	9
				1.23(61)	3.165(1)	0.014(2)		
380	5.04(28)	2.409(4)	0.011(1)	2.94(69)	3.166(6)	0.015(2)	26.01	7
390	5.28(30)	2.408(4)	0.011(1)	3.24(70)	3.170(5)	0.015(2)	26.48	7
410	5.09(29)	2.406(4)	0.011(1)	3.23(69)	3.170(5)	0.015(2)	26.17	7
420	5.17(30)	2.405(4)	0.012(1)	3.37(75)	3.170(5)	0.016(2)	26.99	7
430	5.20(31)	2.407(4)	0.012(1)	3.16(72)	3.172(6)	0.015(2)	27.80	7
440	5.19(32)	2.406(4)	0.012(1)	3.35(81)	3.171(6)	0.016(3)	28.67	7
450	5.55(24)	2.405(3)	0.013(1)	3.95(64)	3.171(4)	0.018(2)	19.89	7

N = Coordination number, r = interatomic distance, A = Debye–Waller factor, R = discrepancy index and N_p = number of independent parameters refined. Note: no errors are quoted for A_{Mo} (values in italics above) for the Mo shell at *ca.* 2.8 Å for the temperature range 100–370 °C because they were calculated using eqns. (1) and (2) (see text).

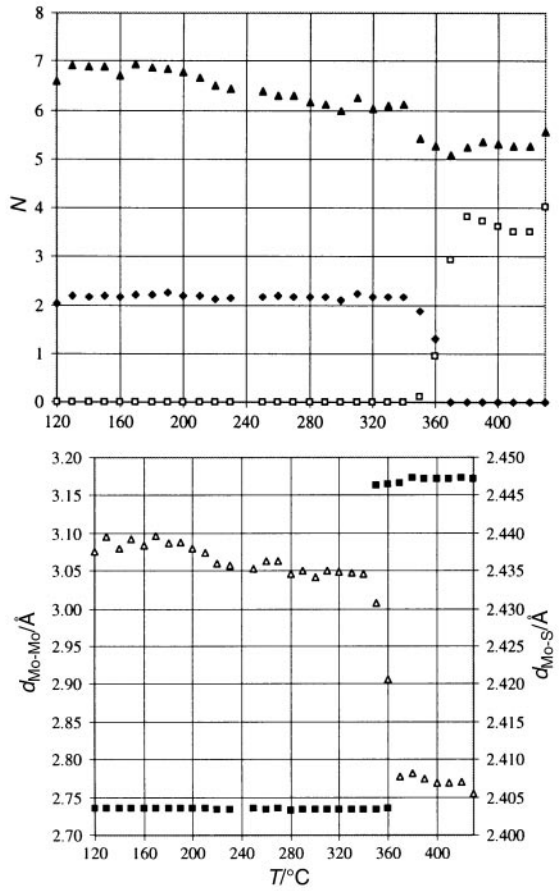

Fig. 6 (Top) coordination number (N) *vs.* temperature for the thermal decomposition of $(NH_4)_2Mo_3S_{13}\cdot 2H_2O$ (Model B) [▲]=N_S, [◆]=N_{Mo} (2.73 Å); [□]=N_{Mo} (3.17 Å) and (bottom) interatomic distances *vs.* temperature for the thermal decomposition of $(NH_4)_2Mo_3S_{13}\cdot 2H_2O$ (Model B) [■]=d_{Mo-Mo}; [△]=d_{Mo-S}, over the temperature range 120–430 °C at a heating rate of 1 °C min^{-1}.

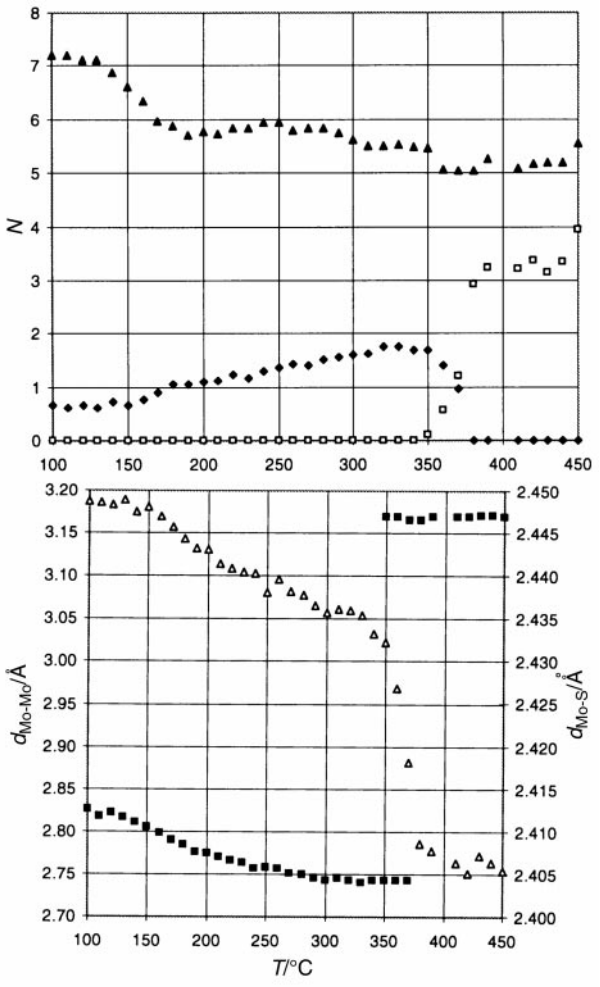

Fig. 7 (Top) coordination number against temperature for the thermal decomposition of $(NH_4)_2Mo_2S_{12}\cdot 2H_2O$ (Model B) [▲]=N_S; [◆]=N_{Mo}(at 2.8 Å); [□]=N_{Mo}(at 3.1 Å) and (bottom) interatomic distances against temperature for the thermal decomposition of $(NH_4)_2Mo_2S_{12}\cdot 2H_2O$ (Model B) [■]=d_{Mo-Mo}; [△]=d_{Mo-S}, over the temperature range 100–450 °C at a heating rate of 1 °C min^{-1}.

the formation of Mo_3S_{12} built from Mo_3 equilateral triangles with S_2 units bridging each side and with a terminal S_2 group on each molybdenum atom. At around 350 °C, the Mo–S coordination number falls towards 5 as poorly crystalline MoS_2 is formed. Fig. 6 (bottom) shows that the bonded Mo–Mo distance hardly changes, remaining around 2.73 Å, until decomposition to MoS_2 occurs at around 350 °C, when a second molybdenum shell corresponding to the non-bonded Mo–Mo distance of 3.16 Å appears. The behaviour of Mo–S distances is more interesting, with a shortening occurring at 200 °C when the apical S is lost from the cluster anion and a further dramatic shortening to 2.41 Å when MoS_2 is formed.

$(NH_4)_2Mo_2S_{12}\cdot 2H_2O$. Fig. 7 (top) shows the behaviour of the average coordination numbers of molybdenum (N_{Mo}) and sulfur (N_S) around molybdenum in $(NH_4)_2Mo_2S_{12}$ and its decomposition products as a function of temperature using model B to fit the EXAFS data. There is a dramatic fall in the Mo–S coordination number around 150 °C. This is consistent with the loss of two of the bridging sulfur atoms per cluster anion $Mo^{v}{}_2S_{12}{}^{2-}$ to form $Mo^{iv}{}_2S_{10}{}^{2-}$ cluster anions. This process is complete when the temperature reaches 200 °C. The average Mo–Mo coordination number appears to start to rise at around 150 °C, and Fig. 7 (bottom) shows that the average Mo–Mo distance falls. These changes are consistent with the conversion of Mo^{v} to Mo^{iv}, which is formed as S_2 is lost from the dimer and electrons are transferred from the $S_2{}^{2-}$ groups to the molybdenum ions. The apparent change in the Mo–Mo coordination number is not real, but reflects the fact that the Mo^{iv}–Mo^{iv} bond is stronger than the Mo^{v}–Mo^{v} bond, and the calculated A_{Mo-Mo} (derived for Mo^{iv}–Mo^{iv} bonds) is too low at the start of the reaction. Above 200 °C, Mo_2 dimers begin to condense to form Mo_3 triangles typical of Mo(IV) containing materials. The condensation reaction continues until 350 °C.

From 200–280 °C the Mo–S coordination number remains at 6, whilst Mo_2 dimers condense to form Mo_3 triangles and NH_3 and H_2S are lost. Some terminal S_2 groups must become bridging S_2 groups during the condensation reaction to form a species similar to the Mo_3S_{12} groups formed by $(NH_4)_2Mo_3S_{13}$, but with S^0 inserted into some of the S_2 groups. Above 300 °C, the Mo–S coordination number begins to fall, as some of the S connected directly to Mo is lost, and at 350 °C MoS_2 begins to form.

MoS_2. The interatomic distances, coordination numbers and Debye–Waller factors found from the EXAFS analysis for the poorly crystalline MoS_2 formed in the two reactions are similar. The coordination numbers found for S and Mo of ~5.5 and 4 are lower than those expected for the crystalline solid in which they are both 6. These values reflect both the small particle size and high degree of disorder in the material formed, and are typical for MoS_2 formed at low temperatures.[7]

IR

$(NH_4)_2Mo_3S_{13}\cdot 2H_2O$. Fig. 8 (top) shows the S–S and Mo–S stretching regions of the IR spectra collected on $(NH_4)_2Mo_3S_{13}\cdot 2H_2O$ at room temperature, and on the decomposition

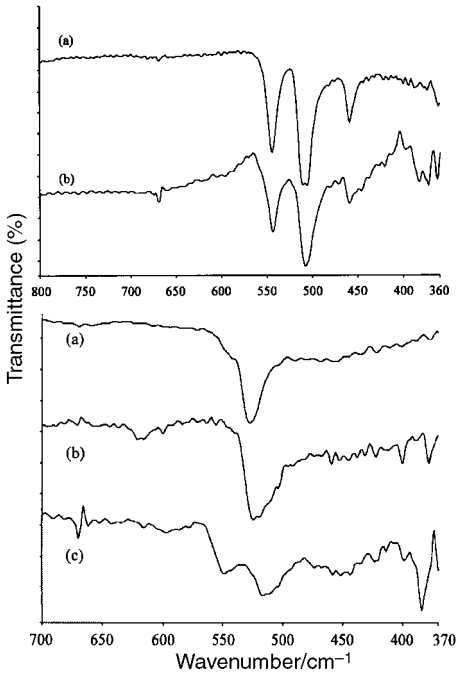

Fig. 8 Expansions of the (S–S) and (Mo–S) stretching regions of the IR spectra of (top) (a) $(NH_4)_2Mo_3S_{13}\cdot 2H_2O$ and (b) the solid product produced by heating the cluster to 370 °C under flowing N_2 and (bottom) of the solid product produced by heating $(NH_4)_2Mo_2S_{12}\cdot 2H_2O$ (a) to (b) 190 °C and (c) 315 °C overnight. Spectra recorded as KBr pellets.

product prepared by heating to 370 °C under flowing N_2 at 10 °C min^{-1}. Under these conditions, a mass loss of 10% has occurred, and the composition is close to $(NH_4)_2Mo_3S_{12.5}$. The bands at 510 and 545 cm^{-1} are assigned to terminal and bridging S_2 groups on the Mo_3 triangles and the band at 459 cm^{-1} to ν(Mo–μ_3-S).[23,24] The latter band has decreased in intensity in agreement with the EXAFS results, which showed a decrease in the Mo–S coordination number consistent with loss of this apical sulfur atom.

$(NH_4)_2Mo_2S_{12}\cdot 2H_2O$. IR spectra were collected on $(NH_4)_2Mo_2S_{12}\cdot 2H_2O$ at room temperature, and on its decomposition products after heating at 190 and 315 °C for 16 h. The relative intensities of the peak at around 1400 cm^{-1} due to the $\delta(NH_4^+)$ vibration for the ammonium ion, and the peak at around 530 cm^{-1} due to the S–S stretch[23] were little changed after heating to 190 °C. This demonstrates that S_2 groups rather than NH_3 and H_2S are lost on heating $(NH_4)_2Mo_2S_{12}$ to 190 °C in agreement with the conclusion from the EXAFS analysis. Fig. 8 (bottom) shows an expansion of the S–S and Mo–S stretching region of the IR spectra. The broadening and shift of the S–S stretching bands at around 530 cm^{-1} on heating to 190 °C are consistent with the formation of the dimer anion, $Mo_2S_{10}^{2-}$. There are more dramatic changes on further heating to 315 °C, and the splitting of the S–S stretches into two distinct groups at 510 and 545 cm^{-1} in the IR spectrum is reminiscent of the spectrum obtained for $(NH_4)_3Mo_3S_{13}$, which has bands at 510 and 545 cm^{-1} assigned to terminal and bridging S_2 groups. This provides further evidence for the formation of Mo_3 trimers.

Conclusions

Schemes for the thermal decomposition reactions of $(NH_4)_2Mo_3S_{13}\cdot 2H_2O$, (Fig. 9), and $(NH_4)_2Mo_2S_{12}\cdot 2H_2O$, (Fig. 10), can be constructed by combining the results of *in situ* EXAFS and X-ray diffraction studies with the results from thermal analysis and IR spectroscopy. On heating under nitrogen, $(NH_4)_2Mo_3S_{13}\cdot 2H_2O$ first loses water with little change in structure. This is followed by loss of H_2S and NH_3 and removal of the apical sulfur from the $Mo_3S(S_2)_6^{2-}$ units to form Mo_3S_{12} units. These triangular units then aggregate to form poorly crystalline MoS_2, *via* the loss of 6 equivalents of sulfur and Mo–Mo bond cleavage. No evidence to corroborate the formation of the intermediate $Mo_6S_{25}^{2-}$ complex ion (Fig. 2) proposed by Müller *et al.*[9] is seen. The complex $(NH_4)_2Mo^{V}_2S_{12}\cdot 2H_2O$ after dehydration undergoes an internal redox reaction with elimination of S_2^0 to form $(NH_4)_2Mo^{IV}_2S_{10}$. A similar reaction has been found to occur on heating $Cs_2Mo_2S_{12}\cdot 2H_2O$ when Müller observed the formation of S_2 molecules.[25,26] This amorphous product then undergoes a remarkable solid-state reaction to form triangular Mo_3 metal–metal bonded units in a material of approximate composition $Mo_3S_{13.5}$. Finally, the Mo_3 units react to form MoS_2 at 350 °C, the same temperature as was found for the condensation of Mo_3S_{12} units, with elimination of sulfur.

Both the very poorly crystalline Mo_3S_{12} (MoS_4) and the amorphous $Mo_3S_{13.5}$ ($MoS_{4.5}$) molybdenum sulfides, formed as intermediates in the decomposition of $(NH_4)_2Mo_3S_{13}\cdot 2H_2O$ and $(NH_4)_2Mo_2S_{12}\cdot 2H_2O$, respectively, contain Mo–Mo bonded Mo^{IV}_3 triangles with bridging and terminal S_2^{2-} groups. It appears that Mo^{IV}_3 triangles are a ubiquitous feature in amorphous molybdenum sulfides. Indeed, we recently had cause to re-examine the structure of amorphous MoS_3 and concluded from a chemical study that around 75% of the molybdenum in this material is found in Mo_3 triangular clusters.[27]

It has been suggested that MoS_4 made by decomposing $(NH_4)_2Mo_2S_{12}\cdot 2H_2O$ in a vacuum consists of chains of $Mo^{IV}S_8$ units linked by face sharing, and that on the basis of theoretical calculations there are no Mo–Mo bonds.[6] However, no experimental evidence was presented to support this proposed structure, which appeared implausible even before the study we

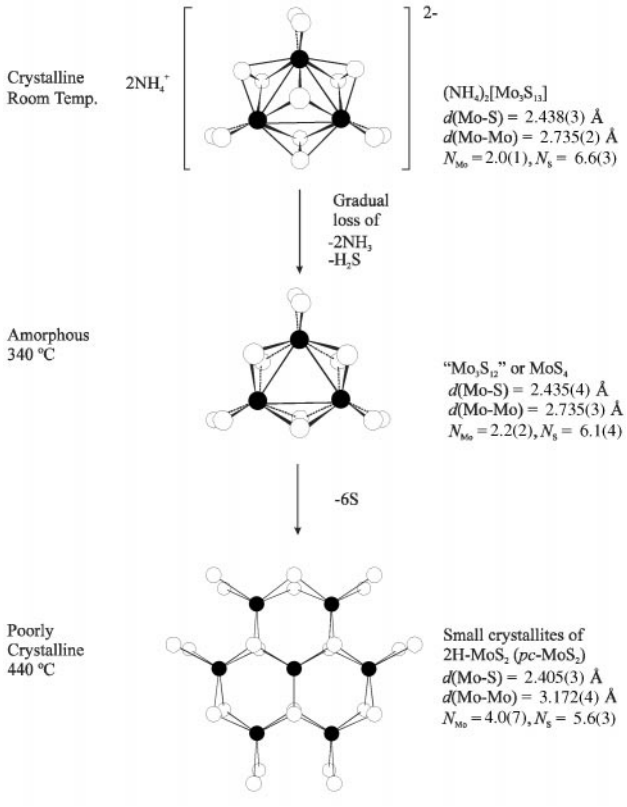

Fig. 9 A schematic representation of the thermal decomposition of the ammonium thiomolybdate $(NH_4)_2Mo_3S_{13}\cdot 2H_2O$, filled circles = Mo, unfilled circles = S.

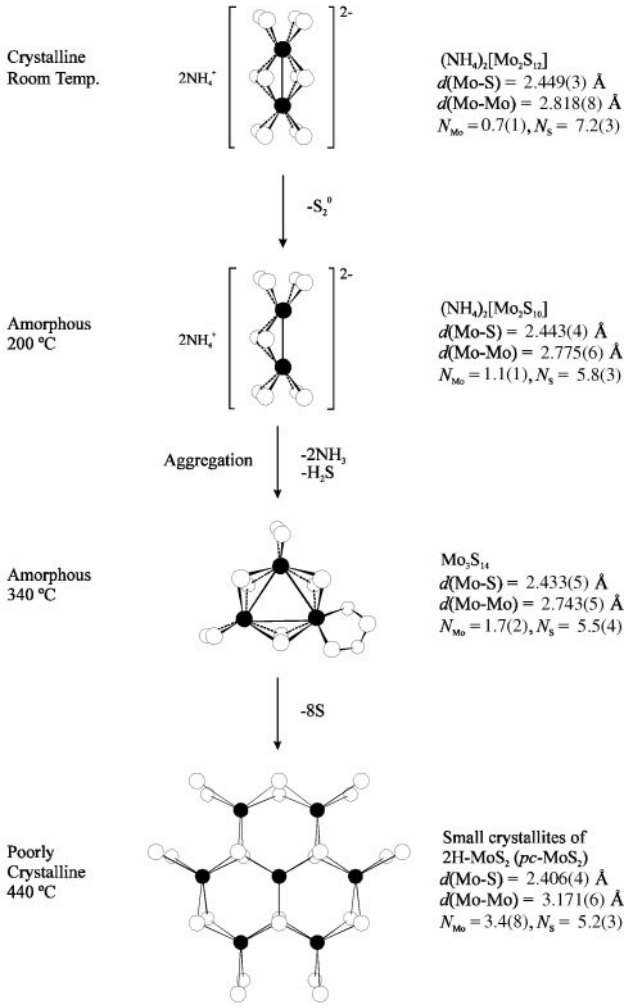

Fig. 10 A schematic representation of the thermal decomposition of the ammonium thiomolybdate $(NH_4)_2Mo_2S_{12}\cdot 2H_2O$, filled circles = Mo, unfilled circles = S.

report here, which must cast further doubt on that work. It seems unlikely that the MoS_4 formed in that experiment had a completely different structure to those found here for MoS_4 and $MoS_{4.5}$. The amorphous sulfide, $MoS_{4.5}$, has a composition close to that of the amorphous sulfide, $MoS_{4.7}$, which we prepared by the reaction of molybdenum hexacarbonyl with sulfur.[13] We concluded in a previous EXAFS study that $MoS_{4.7}$ contained Mo–Mo bonded units,[13] but proposed a chain structure based on molybdenum trimers rather than Mo_3 triangles. The results of this work suggest that the structure of $MoS_{4.7}$ should be re-examined.

Acknowledgements

We thank the EPSRC for the studentship for MRF and Dr I. Harvey for assistance with the *in situ* EXAFS/XRD experiments at Daresbury.

References

1 B. K. Miremadi, K. Colbow and S. R. Morrison, *J. Appl. Phys.*, 1997, **82**, 2639 and references therein.
2 J. C. Muijsers, T. Weber, R. M. van Hardeveld and H. W. Zandbergen, *J. Catal.*, 1995, **157**, 698.
3 T. Weber, J. C. Muijsers, H. van Wolput, C. P. J. Verhagen and J. W. Niemantsverdriet, *J. Phys. Chem.*, 1996, **100**, 14144.
4 A. J. Jacobson, R. R. Chianelli and M. S. Whittingham, *J. Electrochem. Soc.*, 1979, **120**, 2277.
5 R. R. Chianelli, *Int. Rev. Phys. Chem.*, 1982, **2**, 127.
6 G. F. Khudorozhko, L. G. Bullusheva, L. N. Mazalov, V. E. Fedorov, J. Morales, E. A. Kravtsova, I. P. Asanov, G. P. Parygina and Yu. V. Mironov, *J. Phys. Chem. Solids*, 1998, **59**, 283.
7 R. I. Walton, A. J. Dent and S. J. Hibble, *Chem. Mater.*, 1998, **10**, 3737.
8 A. Müller, *Polyhedron*, 1986, **5**, 323.
9 A. Müller, E. Diemann and P. J. Z. Aymonino, *Anorg. Allg. Chem.*, 1981, **479**, 191.
10 A. Müller, W. O. Nolte and B. Krebs, *Inorg. Chem.*, 1980, **19**, 2835.
11 J. L. Brito, M. Ilija and P. Hernández, *Thermochim. Acta*, 1994, **256**, 325.
12 V. P. Fedin, B. A. Kolesov, Y. V. Mironov, O. A. Gerasko and V. E. Fedorov, *Polyhedron*, 1991, **10**, 997.
13 S. J. Hibble, D. A. Rice, D. M. Pickup and M. P. Beer, *Inorg. Chem.*, 1995, **34**, 5109.
14 A. Leist, S. Stauf, S. Löken, E. W. Finckh, S. Lüdtke, K. K. Unger, W. Assenmacher, W. Mader and W. J. Tremel, *J. Mater. Chem.*, 1998, **8**, 241.
15 A. Müller and E. Krickemeyer, *Inorg. Synth.*, 1990, **27**, 47.
16 J. W. McDonald, G. D. Friesen, L. D. Rosenhein and W. E. Newton, *Inorg. Chim. Acta*, 1983, **72**, 205.
17 G. Sankar, P. A. Wright, S. Natarajan, J. M. Thomas, G. N. Greaves, A. J. Dent, B. R. Dobson, C. A. Ramsdale and R. H. Jones, *J. Phys. Chem.*, 1993, **97**, 9550.
18 M. Epple, G. Sankar and J. M. Thomas, *Chem. Mater.*, 1997, **9**, 3127.
19 EXCALIB: Daresbury Laboratory Computer Program.
20 M. Newville, P. Livins, Y. Yacoby, E. A. Stern and J. J. Rehr, *Phys. Rev. B*, 1993, **47**, 14126.
21 N. Binsted, EXCURV98: CCLRC Daresbury Laboratory, 1998.
22 B. K. Teo, *EXAFS: Basic Principles and Data Analysis*, Springer, Berlin, 1986.
23 V. P. Fedin, B. A. Kolesov, Y. V. Mironov and V. Y. Fedorov, *Polyhedron*, 1989, **8**, 2419.
24 A. Müller, S. Sarkar, R. G. Bhattacharyya, S. Pohl and M. Dartmann, *Angew. Chem., Int. Ed. Engl.*, 1978, **17**, 535.
25 A. Müller, W. Jaegermann and J. H. Enemark, *Coord. Chem. Rev.*, 1982, **46**, 245.
26 A. Müller and W. Jaegermann, *Inorg. Chem.*, 1979, **18**, 2631.
27 S. J. Hibble, M. R. Feaviour and M. J. Almond, *J. Chem. Soc., Dalton Trans.*, 2001, 935.